PAPER • OPEN ACCESS

Searching for order in atmospheric pressure plasma jets

To cite this article: Jan Schäfer *et al* 2018 *Plasma Phys. Control. Fusion* **60** 014038

View the article online for updates and enhancements.

IOP Publishing

Searching for order in atmospheric pressure plasma jets

Jan Schäfer[1] , **Florian Sigeneger**[1], **Jiří Šperka**[2] , **Cornelia Rodenburg**[3] and **Rüdiger Foest**[1]

[1] Leibniz Institute for Plasma Science and Technology, Greifswald, Germany
[2] Czech Metrology Institute, Brno, Czech Republic
[3] Department of Materials Science and Engineering, University of Sheffield, United Kingdom

E-mail: jschaefer@inp-greifswald.de

CrossMark

Abstract

The self-organized discharge behaviour occurring in a non-thermal radio-frequency plasma jet in rare gases at atmospheric pressure was investigated. The frequency of the azimuthal rotation of filaments in the active plasma volume and their inclination were measured along with the gas temperature under varying discharge conditions. The gas flow and heating were described theoretically by a three-dimensional hydrodynamic model. The rotation frequencies obtained by both methods qualitatively agree. The results demonstrate that the plasma filaments forming an inclination angle α with the axial gas velocity u_z are forced to a transversal movement with the velocity $u_\phi = \tan(\alpha) \cdot u_z$, which is oriented in the inclination direction. Variations of u_ϕ in the model reveal that the observed dynamics minimizes the energy loss due to convective heat transfer by the gas flow. The control of the self-organization regime motivates the application of the plasma jet for precise and reproducible material processing.

Keywords: plasma jet, self-organization, hydrodynamic simulation

(Some figures may appear in colour only in the online journal)

1. Introduction

The broad variety of material processing ranging from surface treatment, thin film synthesis to in-flight nanoparticle synthesis has driven the development of different plasma jet designs both nowadays and in the past. In this context, non-thermal atmospheric pressure plasma jets (nt-APPJ) have been subject to numerous scientific studies during the last decade. They instantiate a unique combination of interesting properties regarding high chemical reactivity or gas dynamics in a localized region under normal pressure conditions. At the same time, due to their non-thermal character [1] they exert only a limited thermal strain to exposed surfaces. Thanks to these properties manifold applications have been reported in the past and new ideas for beneficial use of these sources keep coming-up constantly.

Historically, applications were related mostly to diverse material processing methods. Already in 1988, a hollow cathode radiofrequency (RF) jet was applied for fluorination and carbon film deposition at atmospheric pressure [2]. Later on, the first jet operating in both gaseous and liquid environment in laboratory conditions was constructed for the treatment of ancient artefacts [3]. The successful reduction of oxidized metal surfaces (e.g. from antique bronze coins [3]) as well as the generation of atomic oxygen for polyimide etching [4] or chemical vapour deposition (CVD) of SiO_2 coatings [5] has triggered a thriving progress of plasma jet devices. Nowadays, several technical solutions and lab-devices exist, which differ largely in dimension, configuration of applied electrical field, power density, materials and geometries. Topical overviews are given e.g. by Lu *et al* [6] and more recently by Reuter *et al* [7]. The investigation of the interaction of plasma jets with biological targets has culminated in the inauguration of plasma medicine as a new
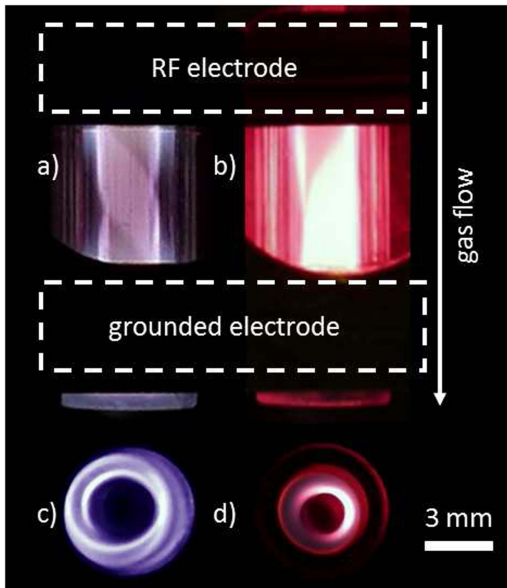
Figure 1. Photographs of locked modes in Ar (a), (c) and Ne (b), (d). The trace of the filaments becomes visible due to longer exposure time ($\approx$0.1 s).

Figure 2. RF plasma jet operating in argon with three rotating filaments (LM3).

discipline in medical research [8]. Notable new developments involve also the treatment of fibres [9] or the implementation of a jet as a preparation technique for scanning electron microscopy [10].

The application of nt-APPJs for homogeneous surface treatment, such as activation of polymer surfaces, cleaning and thin film deposition [11] is still hampered by the presence of steep local gradients of the plasma parameters due to the chaotic (erratic) nature of the filamented discharge channels (plasma filaments). Their formation in a discharge gap is usually a random function of time and an averaging of spatial filament distribution can be only achieved considering longer time intervals. In contrast, collective filament interactions can induce regular operation regimes which in consequence influence the energy dissipation and contribute to a better control of jet operation.

This prediction embodies the basic motivation of the current study. After the observation of a self-organized regime of a plasma jet in 2006, coined with the term 'locked mode' (LM) [12], several further studies were devoted to the properties of the jet, its particular operating regimes, plasma parameters and plasma chemistry during plasma enhanced CVD using organic compounds [13–18]. However, the mechanisms of the LM remain still not fully understood. The plasma jet driven in LM forms equidistantly arranged filaments (Turing pattern) located around the inner capillary wall whereupon the filaments rotate around the symmetry axis of the capillary with frequencies suggesting a decisive role of thermal forces (figure 1). This phenomenon was observed in krypton, argon and neon, but not in helium. Considerations regarding the source of the effect could seize parallels from complex fluid dynamics as e.g. linear vortex shedding described by Strouhal number [19], symmetric travelling waves in pipe flow [20], oscillations due to the Kelvin–
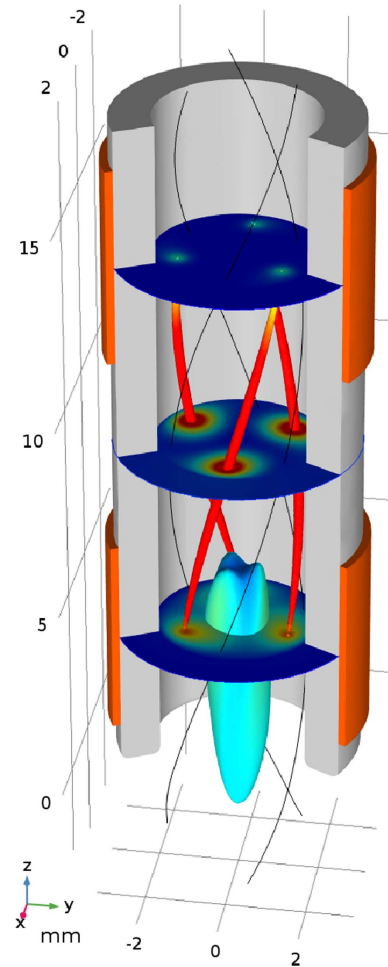
Helmholtz instability [21], Langmuir circulation [22] and result in a modified case of a Taylor–Couette flow [23]. From the plasma physics perspective, several related studies are also relevant for consideration. Equidistant patterning has been observed in dielectric barrier discharges [24]. In a microwave plasma jet a spiral dynamics has been observed with a typical frequency range similar to the RF jet [25].

Because of the complex mechanisms and different temporal and spatial scales, the investigation of the plasma-flow interaction leading to self-organization such as the observed LMs remains a challenging task. In the framework of this study, we attempt to tackle this task by a systematic investigation of the flow dynamics and neutral gas temperature in the LM by means of laser schlieren deflectometry (LSD) [26] and by a three-dimensional hydrodynamic modelling of the plasma jet which approximates the plasma action by heat profiles embedded in the gas volume.

2. Plasma source and methods

The investigations have been performed using the non-thermal capacitively coupled RF plasma jet shown in figure 2.
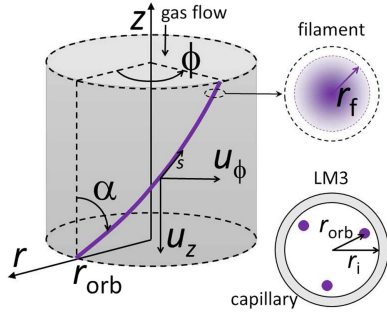
Figure 3. Coordinate system describing the dynamics of the filament.

The RF plasma jet is composed of a quartz capillary with an inner diameter of 4 mm and an outer diameter of 6 mm. Two outer ring electrodes (width 5 mm, distance 5 mm) are adjusted concentrically with the capillary axis. The discharge operates at a frequency of 27.12 MHz in pure argon with a flow rate Q_1 between 0.4 and 0.8 slm. Filaments in different configurations are generated in the active plasma region between both electrodes. The applied power ranges from 7 to 9 W. The inner capillary normally used to inject precursor into the effluent [12] was not used in the current study.

The filament behaviour has been visualized optically by means of a camera (μ digital 800, Olympus). The number of filaments, their positions and inclination angles were determined by data processing of photographs in different discharge conditions. The frequency of filament rotation as well as the gas temperature were measured by LSD [26] in the effluent.

3. Searching for a stationary solution

Our starting hypothesis is that the helical shape of a single filament reflects a tendency of the system to conserve the gas temperature inside the filament over a longer time. Indeed, the gas temperature is in equilibrium with the excited atoms and ions in the filament. Their inertia and live times stabilize the discharge channel beyond the time scale of the RF period. Therefore, the spatial coupling of the filament to its temperature profile represents an optimum, sustaining the energy flux and the gas temperature, too.

If this is a characteristic property of the LM, then the temperature field T can be assumed to fulfil the stationary solution in the helical coordinate system fixed to the moving filament
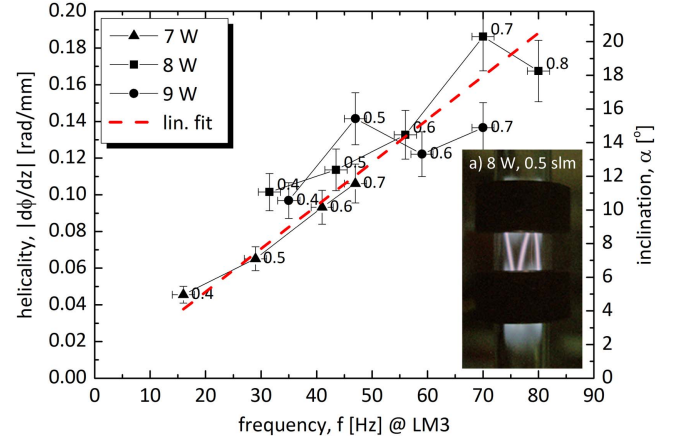
$$\frac{\mathrm{d}T(\mathbf{r}')}{\mathrm{d}t} = 0. \tag{1}$$

The transformation from the laboratory system to the helical coordinate system of the filament ($\mathbf{r}(r, \phi, z) \rightarrow \mathbf{r}'(r', \phi', z')$) is given by following equations:

$$r' = r, \tag{2}$$

$$\phi' = \phi + \omega t, \tag{3}$$

$$z' = z + u_z t, \tag{4}$$

Figure 4. Correlation of helicality or inclination and rotation frequency of filaments in LM3. The point labels denote the flow rate in slm. The photograph of an example (a) demonstrates the filament inclination $\alpha = 12°$ (helicality 0.11 rad mm^{-1}).

where ω is the observed angular velocity of the filament (LM velocity) and u_z is the axial gas velocity. For the definition of the coordinates see figure 3.

By substituting equations (2)–(4) in (1) we obtain a linear relation for the angular velocity:

$$\omega = \frac{u_\phi}{r} = -\frac{\partial \phi'}{\partial z'} u_z = -\frac{\tan \alpha}{r} u_z, \tag{5}$$

where $\partial \phi'/\partial z'$ denotes the helicality of the filament and α is the inclination angle of the filament with the unit vector $\mathbf{z}^0$. Note that the considerations predict the movement of filaments in the direction of the inclination and in the right-handed system $\mathbf{u}_z$ is $(0, 0, -u_z)$. The validity of the hypothesis has been tested experimentally by a systematic variation of RF power, gas flow, and electrode distance. All these implicit parameters cause variations of the LM frequency and of the inclination angle, too. The results are shown in figure 4 and they demonstrate a linear correlation of the frequency and the angular inclination as derived in equation (5).

Despite the simple deduction and the verification, some aspects have been omitted in the present consideration, e.g. the presence of a radial velocity profile and its role in the LM at different axial positions in the jet. Therefore, the hydrodynamic modelling of the jet as well as experimentally investigations of the LM including the related velocity and temperature profiles are required and considered in the following sections.

4. Hydrodynamic model

The flow velocity $\mathbf{u}$ of the gas and its temperature T were determined by solving the hydrodynamic equations of the gas

$$\nabla \cdot (\rho \mathbf{u}) = 0, \tag{6}$$

$$\rho (\mathbf{u} \cdot \nabla) \mathbf{u} = -\nabla p$$
$$+ \nabla \cdot \left(\mu (\nabla \mathbf{u} + (\nabla \mathbf{u})^T) - \frac{2}{3} \mu (\nabla \cdot \mathbf{u}) \mathbf{I} \right), \tag{7}$$

$$\rho\, c_p \mathbf{u} \cdot \nabla T + \nabla \cdot \mathbf{q} = S^{(\mathrm{pl})}, \quad \mathbf{q} = -\lambda(T)\nabla T \qquad (8)$$

which describe the conservation of mass (6), momentum (7) and energy (8) for compressible fluids. Here, ρ denotes the total mass density and p the pressure. The second term on the right-hand side of (7) is deduced from a more general formulation assuming an isotropic fluid with the dynamic viscosity μ. The heat balance equation (8) accounts with the first and second term on the left-hand side for heat convection with the specific heat capacity at constant pressure c_p and for the heat conduction with the heat flux $\mathbf{q}$ and the heat conductivity λ, respectively. The required coefficients for the argon gas have been taken from [27]. A heat conductivity of $\lambda = 1.4 \ \mathrm{W\,m^{-1}\,K^{-1}}$ was used for the capillary quartz glass [28].

The source term $S^{(\mathrm{pl})}$ describes the heating of the gas due to elastic collisions of electrons with gas atoms, due to reactions between heavy particles and due to Joule heating of ions. This quantity could be calculated by a complete plasma model as it was done for an axially symmetric geometry [29]. However, because such a model in three dimensions is a very demanding task, an approximation was used to describe the gas heating from the plasma. Based on investigations of a single filament [17], the power density profile

$$S^{(\mathrm{pl})}(r_{\mathrm{f}}, s) = S^{(\mathrm{pl})}_{\mathrm{max}}\, \Omega(r_{\mathrm{f}})\Theta(s) \qquad (9)$$

depending on the coordinate s along the trace of the filament and on the distance r_{f} from its trace has been deduced. The profile functions $\Omega(r_{\mathrm{f}})$ and $\Theta(s)$ are detailed in [18]. As illustrated in figure 2, the centres of the three filaments occurring in the LM3 mode are positioned on an orbit with radius $r_{\mathrm{orb}} = 1.45$ mm and at the axial position $z_{\mathrm{f}} = 8.5$ mm. Furthermore, the filaments were inclined in azimuthal direction by the angle α. The amplitude $S^{(\mathrm{pl})}_{\mathrm{max}}$ was chosen equal to $5 \times 10^9 \ \mathrm{W\,m^{-3}}$ which is a typical value estimated from prior experimental findings [12].

The Navier–Stokes equations (6)–(8) were solved in a coordinate system which rotates with the rotation frequency $\omega = 2\pi f_{\mathrm{azi}}$ of the filaments. Therefore, the boundary conditions had to be transformed from the lab to the rotating system. The no-slip condition, normally used in the lab system at the wall, changes to the boundary condition $(v_r, v_z, v_\phi) = (0, 0, -r_{\mathrm{cap}}\,\omega\,t)$ and to the condition at the inlet to $(v_r, v_z, v_\phi) = (0, v_z^{\mathrm{in}}(r), -r\,\omega\,t)$ with a parabolic velocity profile $-v_z^{\mathrm{in}}(r) = 2(1 - (r/r_i)^2)v_{\mathrm{max}}$. The maximum velocity v_{max} is deduced from the flow rate at the inlet given as parameter.

With respect to the heat balance equation (8), the temperature was fixed at the electrodes and at the outlet boundaries to $T_0 = 300$ K. At the inlet boundaries, the zero gradient condition $\mathbf{n} \cdot \nabla T = 0$ was applied. At the boundaries adjacent to the electrodes, the ambient radiation was used as boundary condition according to $-\mathbf{n} \cdot \mathbf{q} = \varepsilon_{\mathrm{s}} \sigma_{\mathrm{sb}} (T^4_{\mathrm{amb}} - T^4)$, where σ_{sb} denotes the Stefan–Boltzmann constant, ε_{s} is the surface emissivity of quartz and $T_{\mathrm{amb}} = 300$ K is the ambient temperature.
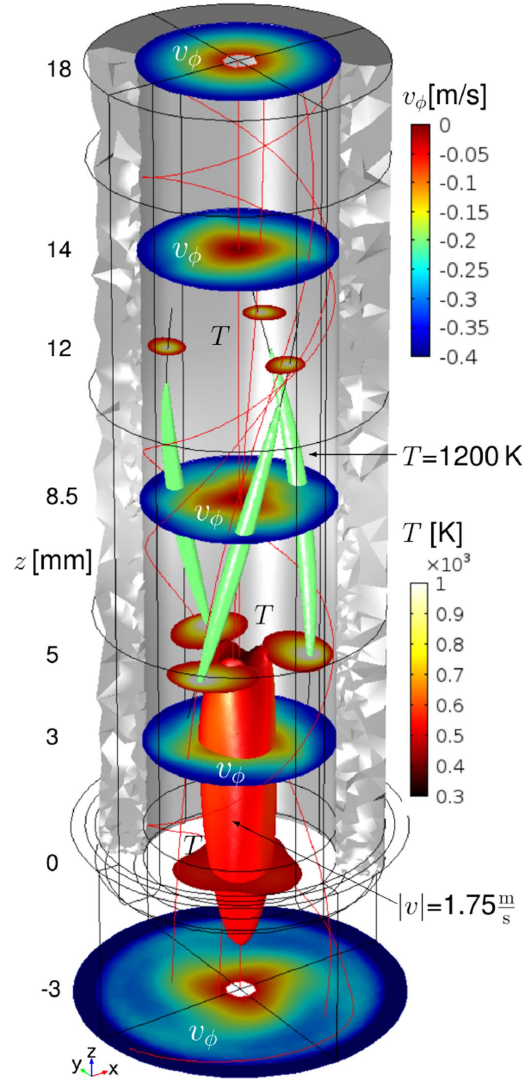

Figure 5. Gas temperature and azimuthal velocity in the plasma jet operating in LM3 mode.

The equation system (6)–(8) was solved using a stationary solver of Comsol Multiphysics. To investigate the influence of the inclination angle and the rotation frequency, the simulations have been performed for a series of parameters. For the inclination angle α the values 8°, 10°, 12°, 16° were used and for each of these values, the rotation frequency was varied. In all cases the gas flow rate amounts to 0.5 slm.

5. Results

As an example, a combined representation of the results for $\alpha = 16°$ and $f = 30$ Hz is shown in figure 5. The position of the three filaments are depicted as green iso-surfaces representing a gas temperature of 1200 K. Furthermore, lateral cuts of the gas temperature are shown at $z = 0$, 5 and 12 mm. Lateral cuts of the azimuthal velocity v_ϕ are shown at $z = -3$, 3, 8.5, 14 and 18 mm. An iso-surface of $|v| = 1.75 \ \mathrm{m\,s^{-1}}$
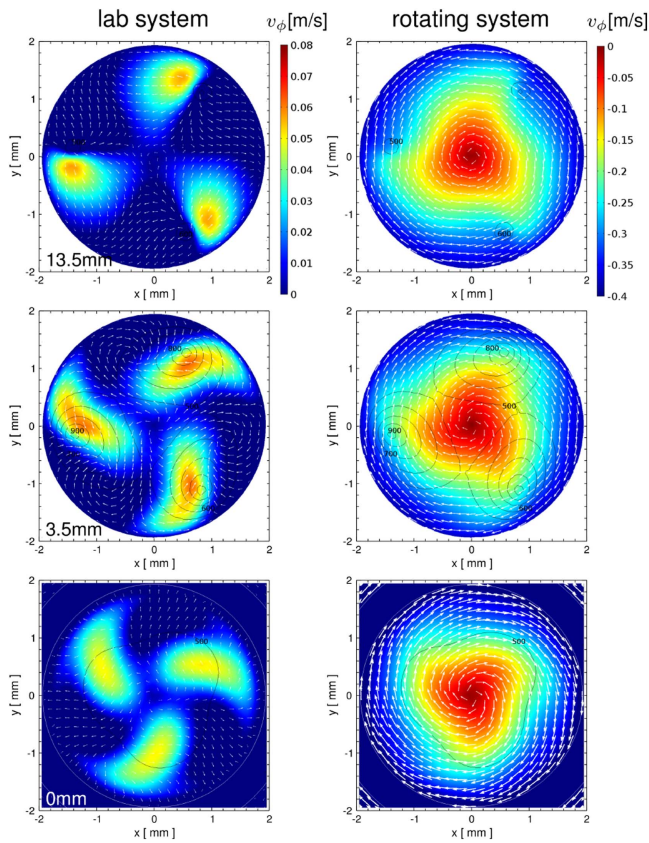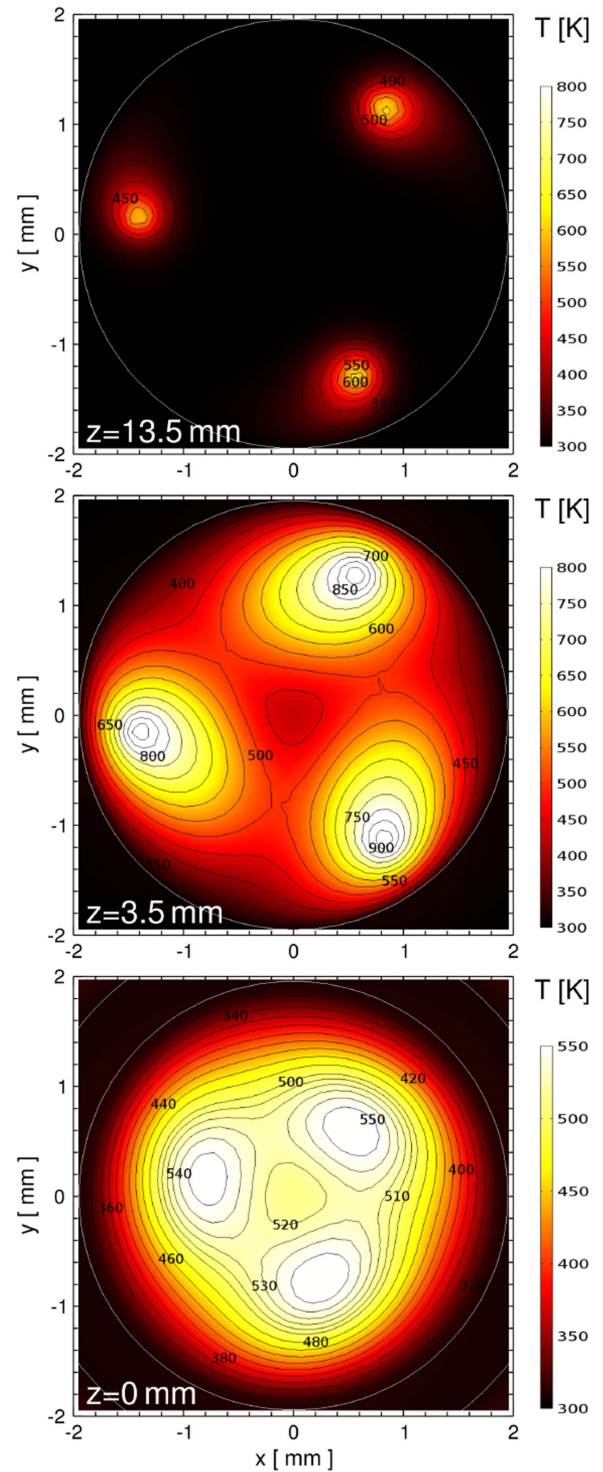
Figure 6. Azimuthal velocity component in the lab system (left) and rotating system (right) for $\alpha = 16°$ and $f = 30$ Hz for three axial positions.

Figure 7. Calculated gas temperature for $\alpha = 16°$ and $f = 30$ Hz.

shows the formation of the plume in the transition from the active plasma region to the effluent. Three streamlines illustrate the shape of the gas flow from the inlet at $z = 18$ mm to the effluent.

The azimuthal velocity component v_ϕ is depicted in figure 6 at three axial positions in the lab and rotating system. Furthermore, this figure contains contour plots of the gas temperature. The action of the boundary condition imposed on the velocity in the rotating system is obvious in the right figures. The contour plots of the gas temperature reveal the asymmetric profile of the filament temperature which is the result of the filament inclination and the azimuthal gas velocity component. In the lab system, three weak vortices establish at $z = 3.5$ mm as shown by the arrows.
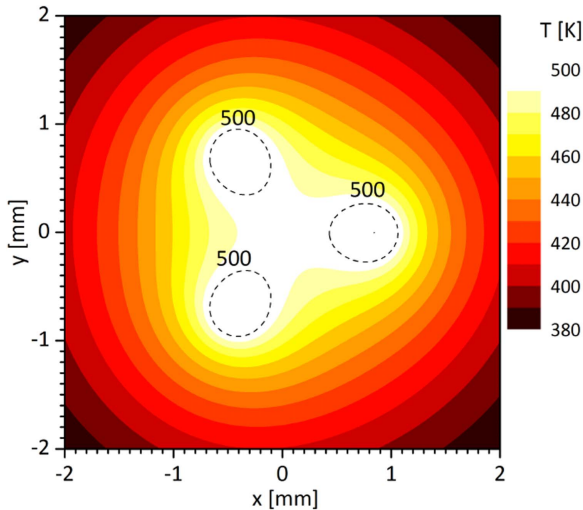
The calculated gas temperature at the same three z positions is shown in figure 7. The series illustrates the evolution of the gas temperature from a position above the active zone ($z = 13.5$ mm) where only a weak tail of the heating profile leads to a slight temperature increase, to a position somewhat below the maximum heating ($z = 3.5$ mm) up to the outlet of the capillary ($z = 0$ mm), where the effluent begins. According to the filament inclination, a torsion of the maximum position can be observed.

Furthermore, the asymmetric contours especially at $z = 3.5$ mm indicate the interplay of heating and convection.

The gas flow transports energy from the active zone into the effluent were temperatures up to 550 K are reached. Due to the overall velocity profile, the energy transport is more pronounced near the centre. Therefore, the distance between the temperature maximum positions at $z = 0$ mm is smaller than at $z = 3.5$ mm. Furthermore, the profiles become more symmetric here indicating that the influence of the azimuthal velocity component diminishes at the outlet position.
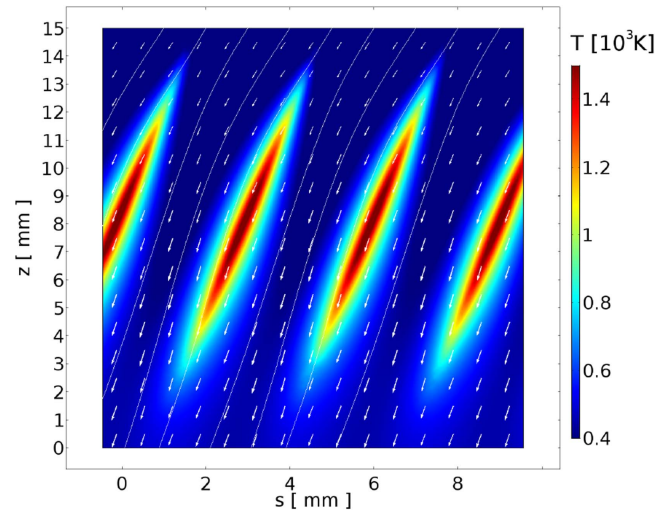
Figure 8. Gas temperature measured at $z = 0$ using the LSD method.

Figure 9. Calculated gas temperature T and velocity direction on the cylinder with radius r_{orb} crossing the filaments.

The temperature profile derived from the LSD measurement at the same position $z = 0$ mm, i.e. at the beginning of the effluent, is shown in figure 8. For the determination of the temperature profile from the measured deflection, the LSD constant of $\delta_0 = 0.53$ mrad was applied [26]. Note, that the corresponding hyperbolic LSD model fits to a stationary analytic solution of the Fourier equation of the heat transport assuming a pure conduction in the gas and the boundary conditions given by maximum laser deflection and by the laboratory temperature. Good qualitative agreement between the modelling and experimental results was obtained at this position. The difference of about 50 K in the maximum temperature can be explained by the uncertainty of the real power values in the plasma.

The gas temperature and the velocity direction obtained on the orbit cylinder with a radius of $r_{orb} = 1.45$ mm are shown in figure 9. The spatial coordinate s denotes the position on this cylinder in azimuthal direction. The shape of the temperature profiles largely coincides with that of the heating profile $S^{(pl)}$ widened by heat conduction. Large differences of up to 700 K between the maxima and minima have been obtained which correspond to pronounced temperature gradients. A closer analysis of the temperature and variation of the rotation frequency reveals the influence of heat convection.

Slight different maximum temperatures, obtained for varying rotation frequency, result from the fact that the convective energy transport is only directed along the filament if the gas velocity direction is parallel to the filament. Because of the influence of the capillary wall, this condition is only fulfilled at a certain rotation frequency. At larger or smaller frequencies, the component of the gas velocity perpendicular to the filament orientation leads to additional convective cooling of the filament. Therefore, the optimal frequency can be determined from the simulation results by detecting the maximum temperature in the plasma jet. These selected points, i.e. the maximum temperature at optimal rotation
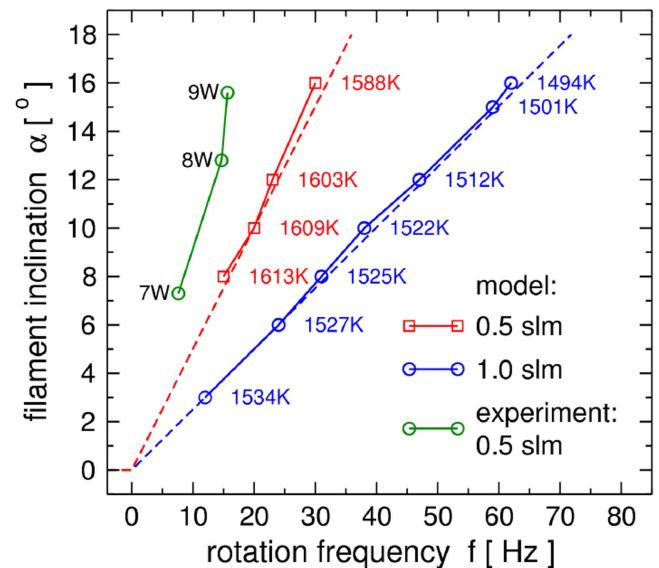
Figure 10. Relation between filament inclination and rotation frequency for modelling and experimental results. The labels denote the power and the calculated global maximum temperature, respectively.

frequency, are indicated as labels in figure 10 for the flow rates 0.5 and 1.0 slm. Moreover, this figure shows the relation between filament inclination and rotation frequency. The linear dependence deduced from the simulations for the flow rates 0.5 and 1.0 slm is mostly confirmed by the experimental results for 0.5 slm. Deviations between the slope obtained experimentally and from the simulation may be caused by the uncertainty about the supplied power. Indeed, a part of the power supplied by the generator is consumed by the matching network driving the RF plasma jet. Therefore, the experimental values can be slightly overestimated, while the inclination and LM frequency are smaller than in the model.

6. Summary

The self-organization of filaments occurring in a non-thermal plasma jet at atmospheric pressure has been investigated. The complex interaction of various physical mechanisms limits the investigation to one aspect of this phenomenon. This aspect refers to the relation between the inclination of the filaments in the capillary and their rotation frequency.

The gas flow and the heating of the gas due to three inclined plasma filaments (LM3) has been investigated by a three-dimensional hydrodynamic model. The model comprises the Navier–Stokes equations for the compressible argon gas and the heat balance equation with heat sources caused by the filaments. The filaments are fixed in the rotating system with a pre-assumed inclination and spatial heating profile. The latter has been determined by previous investigations of a single filament by a detailed plasma model.

The results confirm the linear dependence of the rotation frequency on the inclination angle of the filaments. It has been found that such a rotation frequency is established which leads to a maximum gas temperature. With such an optimal frequency of in the LM, the gas flow around the filaments is parallel to the inclined filaments which minimizes the energy loss due to convective cooling as assumed for a self-organized regime.

The results motivate the application of the locked-mode in processes where a regular and efficient filament dynamics contribute to an enhanced reproducibility of the plasma conditions and hence a better control of the aspired product properties.

Acknowledgment

ORCID iDs

Jan Schäfer https://orcid.org/0000-0002-0652-5057
Jiří Šperka https://orcid.org/0000-0001-6157-4030
Cornelia Rodenburg https://orcid.org/0000-0002-9590-375X

References

[1] Schütze A, Yeong J Y, Babayan S E, Park J, Selwyn G S and Hicks R F 1998 *IEEE Trans. Plasma Sci.* **26** 1685
[2] Kanazawa S, Kogoma M, Moriwaki T and Okazaki S 1998 *J. Phys. D: Appl. Phys.* **21** 838
[3] Klíma M, Zajíčková L and Janča J 1997 *Z. Schweiz. Archäologie Kunstgeschichte* **54** 31
[4] Jeong J Y, Babayan S E, Tu V J, Park J, Hicks R F and Selwyn G S 1998 *Plasma Sources Sci. Technol.* **7** 282
[5] Babayan S E, Jeong J Y, Tu V J, Park J, Selwyn G S and Hicks R F 1998 *Plasma Sources Sci. Technol.* **7** 286
[6] Lu X, Laroussi M and Puech V 2012 *Plasma Sources Sci. Technol.* **21** 034005
[7] Reuter S, Sousa J S, Stancu G D and van Helden J-P H 2015 *Plasma Sources Sci. Technol.* **24** 05400
[8] Weltmann K-D and von Woedtke T 2017 *Plasma Phys. Control. Fusion* **59** 01403
[9] Schäfer J, Horn S, Brandenburg R, Foest R, Stieber M and Weltmann K-D 2012 *Patent No* EP2716139 B1, Germany
[10] Schäfer J 2013 Atmospheric pressure plasma jet improves scanning electron microscopy of non-conductive samples (https://doi.org/10.13140/RG.2.2.23681.66400)
[11] Schäfer J, Fricke K, Mika F, Pokorná Z, Zajíčková L and Foest R 2017 *Thin Solid Films* **630** 71
[12] Schäfer J, Foest R, Quade A, Ohl A and Weltmann K-D 2008 *J. Phys. D: Appl. Phys.* **41** 194010
[13] Schäfer J, Foest R, Ohl A and Weltmann K-D 2009 *Plasma Phys. Control. Fusion* **51** 124045
[14] Schäfer J, Sigeneger F, Foest R, Loffhagen D and Weltmann K-D 2010 *Eur. Phys. J. D* **60** 531
[15] Vogelsang A, Ohl A, Foest R and Weltmann K-D 2013 *Plasma Process. Polym.* **10** 364
[16] Schäfer J, Sigeneger F, Foest R, Loffhagen D and Weltmann K-D 2017 *Eur. Phys. J. D* (https://doi.org/10.1140/epjd/e2017-80364-6)
[17] Sigeneger F and Loffhagen D 2016 *Plasma Sources Sci. Technol.* **25** 035020
[18] Sigeneger F, Becker M M, Foest R and Loffhagen D 2016 *J. Phys. D: Appl. Phys.* **49** 345202
[19] Strouhal V 1878 *Ann. Phys. Chem.* **5** 216
[20] Pringle C C T and Kerswell R R 2007 *Phys. Rev. Lett.* **99** 074502
[21] Walker G T 1932 *Nature* **129** 205
[22] Craik A D D and Leibovich S 1976 *J. Fluid Mech.* **73** 401
[23] Rayleigh J S 1880 *Sci. Pap.* **3** 594
[24] Schoenbach K H, Moselhy M and Shi W 2004 *Plasma Sources Sci. Technol.* **13** 177
[25] Hnilica J, Kudrle V, Vašina P, Schäfer J and Aubrecht V 2012 *J. Phys. D: Appl. Phys.* **45** 055201
[26] Schäfer J, Bonaventura Z and Foest R 2015 *Eur. Phys. J. Appl. Phys.* **71** 20804
[27] Boulos M I, Fauchais P and Pfender E 1994 *Thermal Plasmas: Fundamentals an Applications* vol 1 (New York: Plenum) (https://doi.org/10.1007/978-1-4899-1337-1)
[28] Lide D R (ed) 2010 *CRC Handbook of Chemistry and Physics* vol 90 (Boca Raton, FL: CRC Press)
[29] Sigeneger F, Schäfer J, Weltmann K-D, Foest R and Loffhagen D 2017 *Plasma Process. Polym.* **14** 1600112